The 2009 IEEE/RSJ International Conference on
Intelligent Robots and Systems
October 11-15, 2009 St. Louis, USA

Scaling and Eliminating Non-Contact Forces and Torques to Improve Bilateral Teleoperation

Daniel Kubus and Friedrich M. Wahl

Abstract— **In bilateral teleoperation, the operator experiences forces and torques applied to the slave manipulator. These forces and torques, however, consist of two components: on the one hand, forces and torques due to contacts with the environment, and on the other hand, non-contact forces, i.e., inertial forces, centrifugal forces, Coriolis forces, and associated torques. For several reasons, eliminating these non-contact forces and torques from the force-torque measurements of the slave or scaling them can be advantageous. For instance, in highly-dynamic teleoperation tasks, these forces and torques may contribute to operator fatigue or hamper the detection of contacts with the environment. This paper briefly reviews the estimation of inertial parameters of the slave load, e.g., an end-effector or a gripper. Subsequently, a method for eliminating the non-contact forces and torques from the measurements of a wrist-mounted force-torque sensor or scaling them is presented. After a brief overview of our teleoperation system, experimental results are presented which demonstrate the effectiveness of our approach.**

I. Introduction

In various teleoperator control approaches, feeding forces and torques applied to the slave back to the master plays a key role. Often, wrist-mounted force-torque sensors are used to measure the forces and torques exerted on the slave manipulator. If one looks closely at the forces and torques that are exerted on the slave, two basic components may be distinguished. On the one hand, forces and torques may be caused by contacts with the environment, and on the other hand, non-contact forces-torques result from the inertial properties of the load, i.e., the end effector or gripper attached to the force-torque sensor (and possibly gripped objects). These non-contact forces and torques are composed of inertial forces, centrifugal forces, Coriolis forces, and associated torques.

In teleoperation systems with a non-negligible communication delay, additional forces-torques may arise which are not related to any interaction with the environment or the inertial properties of the load but originate from a controller which stabilizes the system, e.g., when using passivity-based approaches [1]. In this paper teleoperation systems with negligible communication and loop delays are regarded.

Using standard approaches, both contact forces and torques and non-contact forces and torques are fed back to the user. One may now argue, that this contributes to realistic haptic perception but there are several reasons why eliminating these non-contact forces and torques may improve system performance. Firstly, often a gripper is attached to the force-torque sensor which contributes to the non-contact forces and torques exerted on the sensor. The influence of this gripper, however, is not desirable for realistic haptic perception. Secondly, in highly-dynamic teleoperation tasks, frequent acceleration and deceleration of the load contributes to operator fatigue due to the non-contact forces and torques experienced by the operator. Moreover, non-contact forces and torques may complicate certain tasks since the user has to counteract them when moving an object or the end-effector respectively. Thirdly, regarding contacts during highly-dynamic movements, non-contact forces and torques may 'mask' contact forces-torques thus delaying or even preventing the detection of contacts with the environment by the human operator or a controller.

For teleoperated assembly tasks, it may also be desirable to upscale or downscale these non-contact forces and torques to virtually change the apparent mass of the load. Downscaling the non-contact forces-torques or upscaling the contact forces-torques may be preferable to completely removing non-contact forces-torques since users may perform better when the manipulated object does not appear massless – as the mass of an object is an important clue for humans when manipulating or assembling objects. Please consult [2] for a thorough discussion. However, the above assumption has to be validated by experiments that focus on these psychophysical issues.

During the last five decades, numerous control approaches for bilateral teleoperation have been proposed. A comprehensive historical review by Hokayem and Spong [1] has been published recently. Generally, these control approaches intend to guarantee control stability or perceptual stability respectively. Perceptual instability refers to all unrealistic sensations perceived during contacts with the environment which cannot be attributed to the physical properties of the environment – for instance buzzing [3]. In contrast to control stability, perceptual stability is a subjective criterion that involves evaluation by users.

A commonly accepted ultimate goal of teleoperation systems is transparency, i.e., the user does not recognize a difference between interacting with the environment directly or indirectly using the teleoperation system. Transparency, however, should not always be a major design objective. In fact, the contact detection performance of humans can be improved by modifying the forces-torques measured by the force-torque sensor, which are *ideally* identical with those the user would experience when directly interacting with the environment. Regarding highly-dynamic handling and

The authors are with the Institut für Robotik und Prozessinformatik, Technische Universität Braunschweig, 38106 Braunschweig, Germany. {d.kubus, f.wahl}@tu-bs.de

assembly tasks, humans may not be able to perceive contacts with the environment due to significant non-contact forces and torques, e.g., inertial forces, centrifugal forces, Coriolis forces, and associated torques, which result from highly-dynamic movements of the handled object. Therefore, it may be beneficial to eliminate or reduce these non-contact forces and torques when performing a handling or assembly task with teleoperation systems although this modification clearly reduces transparency.

Our approach enables the estimation of the inertial parameters of arbitrary loads attached to the slave manipulator. These parameters may then be used to eliminate or scale the non-contact forces and torques which are fed back to the user. Furthermore, the non-contact forces and torques due to a gripper attached to the slave may be eliminated while the non-contact forces and torques of an attached object are transmitted to the user. Obviously, our approach offers various options to handle non-contact forces and torques in teleoperation. It may be combined with many proposed control approaches for teleoperators, e.g., in our teleoperation system a position-force control architecture with passivity control [4] is employed.

The remainder of this paper is structured as follows: Section II briefly reviews work that is related to the proposed approach. Section III addresses the equations that are necessary to estimate the inertial parameters and to eliminate or scale the non-contact forces and torques. In Section IV approaches to online-estimation of inertial parameters of loads attached to the slave manipulator are briefly reviewed. The elimination and scaling resp. of the non-contact forces and torques is addressed in Section V. Our experimental results which demonstrate the advantages of non-contact force scaling and elimination are presented in Section VI. Section VII concludes the paper and gives an outlook especially addressing psychophysical issues.

II. Related Work

Several teleoperation control approaches consider the compensation of friction, gravity, and inertia of the *slave manipulator* but do not regard the influence of the load explicitly, e.g., [5], [6]. In [7] Lee addressed *scaling* the inertia of a teleoperator system without explicitly considering the inertial parameters of an end-effector or those of gripped objects.

In the field of industrial robotics the estimation of inertial parameters of robot loads has been tackled using different approaches, e.g., employing online estimation [8], [9] or off-line estimation [10]. The elimination of non-contact forces and torques to improve force control performance in industrial applications has also been addressed recently [11]–[14]. In [13], [14] the ten inertial parameters of a load have been used to calculate the non-contact forces and torques and subsequently subtract them from the measurements of a wrist-mounted force-torque sensor to yield *pure* contact forces and torques.

However, both the elimination and scaling of non-contact forces and torques applied to a slave manipulator considering the entire set of inertial parameters of the load has not been addressed yet in the teleoperation literature to the best of our knowledge.

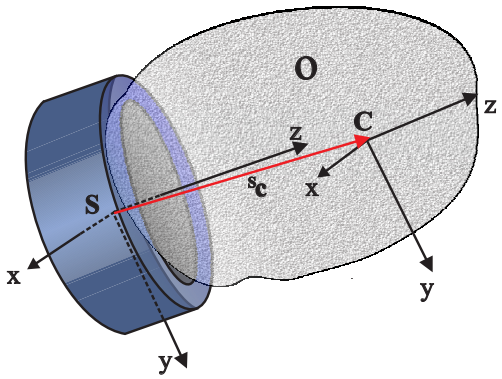

Fig. 1. Force/torque sensor with attached load.

III. Equations for Estimating Inertial Parameters and Calculating Non-Contact Forces and Torques

This section briefly addresses the equations which are employed to estimate the inertial parameters of the load and to calculate the non-contact forces and torques. To estimate the inertial parameters of the load attached to the slave, equations relating the dynamic state of the load and its inertial parameters (mass m, coordinates of the center of mass $\boldsymbol{c}$, and the elements of the inertia matrix $\boldsymbol{I}$) to the forces and torques ${}^S\boldsymbol{f}$,${}^S\boldsymbol{\tau}$ measured by the wrist-mounted force-torque sensor have to be derived from the basic laws of dynamics. Based on the Newton-Euler approach, the motion of a rigid body due to external forces and torques is described by two vector equations, i.e., Eqns. (1) and (2). Fig. 1 depicts the force-torque sensor with a load/object O attached to it. The measured forces ${}^S\boldsymbol{f}$, torques ${}^S\boldsymbol{\tau}$, the linear and angular acceleration vector ${}^S\boldsymbol{a}$ and ${}^S\boldsymbol{\alpha}$, the angular velocity vector ${}^S\boldsymbol{\omega}$, the gravity vector ${}^S\boldsymbol{g}$, the coordinates of the center of mass ${}^S\boldsymbol{c}$, and the inertia matrix ${}^S\boldsymbol{I}$ refer to the sensor frame $\boldsymbol{S}$.

$$ {}^S\boldsymbol{f} = m\,{}^S\boldsymbol{a} - m\,{}^S\boldsymbol{g} + {}^S\boldsymbol{\alpha} \times m\,{}^S\boldsymbol{c} + {}^S\boldsymbol{\omega} \times \left({}^S\boldsymbol{\omega} \times m\,{}^S\boldsymbol{c}\right) \quad (1) $$

$$ {}^S\boldsymbol{\tau} = {}^S\boldsymbol{I}\,{}^S\boldsymbol{\alpha} + {}^S\boldsymbol{\omega} \times \left({}^S\boldsymbol{I}\,{}^S\boldsymbol{\omega}\right) + m\,{}^S\boldsymbol{c} \times {}^S\boldsymbol{a} - m\,{}^S\boldsymbol{c} \times {}^S\boldsymbol{g} \quad (2) $$

where

$$ \boldsymbol{I} = \begin{pmatrix} I_{xx} & I_{xy} & I_{xz} \\ I_{xy} & I_{yy} & I_{yz} \\ I_{xz} & I_{yz} & I_{zz} \end{pmatrix} \quad (3) $$

If one of the mentioned parameters is not measured w.r.t. the frame $\boldsymbol{S}$, it can be readily transformed [15]. Note that the axes of the frame $\boldsymbol{C}$ located at the center of mass (COM) of the object are parallel to the axes of $\boldsymbol{S}$. The matrix equation Eq. (4) used for both parameter estimation and calculation of non-contact forces and torques relates the measured forces ${}^S\boldsymbol{f}$ and torques ${}^S\boldsymbol{\tau}$ as well as the variables ${}^S\boldsymbol{a}$, ${}^S\boldsymbol{\alpha}$, ${}^S\boldsymbol{\omega}$, and ${}^S\boldsymbol{g}$ to the complete set of inertial parameters contained in ${}^S\boldsymbol{\varphi}$.

$$ \begin{pmatrix} {}^S\boldsymbol{f} \\ {}^S\boldsymbol{\tau} \end{pmatrix} = {}^S\boldsymbol{V}\left({}^S\boldsymbol{a}, {}^S\boldsymbol{\alpha}, {}^S\boldsymbol{\omega}, {}^S\boldsymbol{g}\right) {}^S\boldsymbol{\varphi} \quad (4) $$

$$
{}^{S}\boldsymbol{V} = \begin{pmatrix}
a_x - g_x & -\omega_y^2 - \omega_z^2 & \omega_x\omega_y - \alpha_z & \omega_x\omega_z + \alpha_y & 0 & 0 & 0 & 0 & 0 & 0 \\
a_y - g_y & \omega_x\omega_y + \alpha_z & -\omega_x^2 - \omega_z^2 & \omega_y\omega_z - \alpha_x & 0 & 0 & 0 & 0 & 0 & 0 \\
a_z - g_z & \omega_x\omega_z - \alpha_y & \omega_y\omega_z + \alpha_x & -\omega_y^2 - \omega_x^2 & 0 & 0 & 0 & 0 & 0 & 0 \\
0 & 0 & a_z - g_z & g_y - a_y & \alpha_x & \alpha_y - \omega_x\omega_z & \alpha_z + \omega_x\omega_y & -\omega_y\omega_z & \omega_y^2 - \omega_z^2 & \omega_y\omega_z \\
0 & g_z - a_z & 0 & a_x - g_x & \omega_x\omega_z & \alpha_x + \omega_y\omega_z & \omega_z^2 - \omega_x^2 & \alpha_y & \alpha_z - \omega_x\omega_y & -\omega_x\omega_z \\
0 & a_y - g_y & g_x - a_x & 0 & -\omega_x\omega_y & \omega_x^2 - \omega_y^2 & \alpha_x - \omega_y\omega_z & \omega_x\omega_y & \alpha_y + \omega_x\omega_z & \alpha_z
\end{pmatrix} \tag{5}
$$

Eqns. (1) and (2) are used to compose the desired matrix ${}^{S}\boldsymbol{V}$, cf. Eq. (5) [10] at the top of this page. Note that the index ^{S} is omitted in Eq. (5) for the sake of clarity. The parameter vector ${}^{S}\boldsymbol{\varphi}$ contains the complete set of inertial parameters of the load:

$$
\begin{aligned}
{}^{S}\boldsymbol{\varphi} \quad = \quad & \big[m, m\,{}^{S}c_x, m\,{}^{S}c_y, m\,{}^{S}c_z, \\
& {}^{S}I_{xx}, {}^{S}I_{xy}, {}^{S}I_{xz}, {}^{S}I_{yy}, {}^{S}I_{yz}, {}^{S}I_{zz}\big]^T
\end{aligned} \tag{6}
$$

The matrix ${}^{S}\boldsymbol{V}$, as defined above, does not consider an important characteristic of common strain gage force/torque sensors. The forces and torques measured by these sensors typically show time-varying offsets that would deteriorate the estimation results. In order to handle these offsets two approaches may be pursued: Either the sensor values may be zeroed in a known sensor orientation considering the eliminated gravitational forces and associated torques by a pseudo gravity vector or the offsets may be estimated directly [8]. To estimate the force and torque offsets, the matrix ${}^{S}\boldsymbol{V}$ can be augmented by a 6×6 identity matrix $\boldsymbol{E}$ and consequently the parameter vector ${}^{S}\boldsymbol{\varphi}$ is expanded by the force/torque offsets $\boldsymbol{f_o}$, $\boldsymbol{\tau_o}$ to be estimated.

$$
{}^{S}\boldsymbol{\varphi_{ext}} = \big[f_{o_x}, f_{o_y}, f_{o_z}, \tau_{o_x}, \tau_{o_y}, \tau_{o_z}, {}^{S}\boldsymbol{\varphi}\big]^T \tag{7}
$$

$$
{}^{S}\boldsymbol{V_{ext}} = \big[\boldsymbol{E_{6\times 6}}\,{}^{S}\boldsymbol{V}\big] \tag{8}
$$

IV. Estimation Approach

To estimate the inertial parameters of a load, several approaches may be employed, e.g., [8], [10]. Following [8], the manipulator executes a sinusoidal estimation trajectory in joint space, which involves no contacts with the environment. Thus, the forces and torques exerted on the wrist-mounted force-torque sensor are *pure* non-contact forces and torques. A fixed number of N weighted sine and cosine functions are superposed to compose the trajectory of a joint [16], [17]. Following this approach, the trajectory $q_i(t)$ of joint i is given by:

$$
s_i(t) = \sum_{k=1}^{N} \rho_{i,k} \sin(2\pi k f t) + \delta_{i,k} \cos(2\pi k f t) \tag{9}
$$

$$
q_i(t) = s_i(t) + q_{i,0} \tag{10}
$$

where $s_i(t)$ denotes the sinusoidal part. The parameter $q_{i,0}$ denotes a constant offset angle; $\rho_{i,k}$ and $\delta_{i,k}$ are the coefficients of the sine and the cosine part respectively. The base frequency f of the joint trajectories is identical to ensure periodicity. Note that trajectories according to Eq. (10) are jerk-limited (since the derivative of a sinusoidal function is sinusoidal again) and hence reduce undesired excitation of the mechanical structure of the manipulator. The weights $\rho_{i,k}$ and $\delta_{i,k}$ may be optimized w.r.t. a suitable criterion that evaluates the influence of the selected trajectory on the noise and bias sensitivity of the estimates [8].

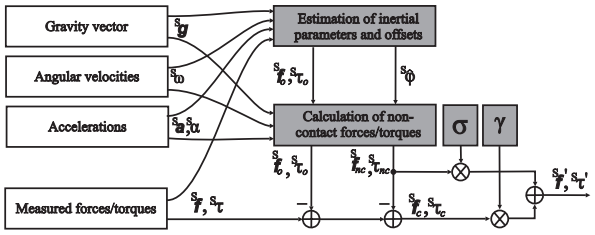

Fig. 2. Schematic representation of the parameter estimation and non-contact force scaling/elimination approach. The parameters σ and γ control the scaling of the non-contact forces-torques and the contact forces-torques resp.

During the execution of the trajectory, the forces ${}^{S}\boldsymbol{f}$ and torques ${}^{S}\boldsymbol{\tau}$ as well as linear accelerations ${}^{S}\boldsymbol{a}$, angular accelerations ${}^{S}\boldsymbol{\alpha}$, and angular velocities ${}^{S}\boldsymbol{\omega}$ have to be measured by dedicated sensors or estimated based on encoder signals [18]. Moreover, the gravity vector ${}^{S}\boldsymbol{g}$ has to be determined. Since acceleration sensors tend to exhibit significant noise and disturbances [19], accelerations may be derived from encoder measurements [8] if sinusoidal excitation according to [16], [17] is employed. Based on the equations presented in Section III the inertial parameters of the load may be estimated. If online estimation of the parameters – i.e., during the execution of the trajectory – is required to accelerate the estimation process, the recursive instrumental variables (RIV) method may be utilized [8]; even better results are achieved with the recursive total least-squares method introduced in [9]. Otherwise, the approach described in [10] may be used as well.

V. Elimination and Scaling of Non-Contact-Forces and Torques

The forces and torques ${}^{S}\boldsymbol{f}$, ${}^{S}\boldsymbol{\tau}$ acting upon the force-torque sensor can be divided into contact forces-torques ${}^{S}\boldsymbol{f_c}$, ${}^{S}\boldsymbol{\tau_c}$ caused by the contact of the load with the environment and inertial, centrifugal, and Coriolis forces as well as associated torques exerted by the load. The latter are called non-contact forces and torques ${}^{S}\boldsymbol{f_{nc}}$, ${}^{S}\boldsymbol{\tau_{nc}}$.

$$
\begin{bmatrix} {}^{s}\boldsymbol{f} \\ {}^{s}\boldsymbol{\tau} \end{bmatrix} = \begin{bmatrix} {}^{s}\boldsymbol{f_{nc}} \\ {}^{s}\boldsymbol{\tau_{nc}} \end{bmatrix} + \begin{bmatrix} {}^{s}\boldsymbol{f_c} \\ {}^{s}\boldsymbol{\tau_c} \end{bmatrix} \tag{11}
$$

Fig. 2 depicts the major components of the estimation and elimination scheme. The blocks on the left symbolize the input signals that are used by both the estimation block and

the calculation block. Following the estimation approaches reviewed in Section IV, the inertial parameters of the load as well as the offsets $\boldsymbol{f_o}$ and $\boldsymbol{\tau_o}$ of the force-torque sensor are estimated during a sinusoidal trajectory. The non-contact forces and torques are calculated using the inertial parameters and the matrix ${}^{S}\boldsymbol{V}$, that relates these estimated parameters ${}^{S}\hat{\boldsymbol{\varphi}}$ to the non-contact forces and torques exerted on the sensor by the load.

$$\begin{bmatrix} {}^{s}\boldsymbol{f_{nc}} \\ {}^{s}\boldsymbol{\tau_{nc}} \end{bmatrix} = {}^{S}\boldsymbol{V}\,{}^{S}\hat{\boldsymbol{\varphi}} \tag{12}$$

If the inertial parameters are expressed w.r.t. $\boldsymbol{C}$, no angular velocity signals are required for the removal or scaling of non-contact forces-torques as described in [13]. If force-torque sensor offsets are also considered when the non-contact forces-torques are removed or scaled, the contact forces-torques at time-step k are computed by subtracting the non-contact forces-torques and the offsets from the forces and torques provided by the force-torque sensor.

$$\begin{bmatrix} {}^{s}\boldsymbol{f_{c,k}} \\ {}^{s}\boldsymbol{\tau_{c,k}} \end{bmatrix} = \begin{bmatrix} {}^{s}\boldsymbol{f_{k}} \\ {}^{s}\boldsymbol{\tau_{k}} \end{bmatrix} - \begin{bmatrix} {}^{s}\boldsymbol{f_{o,k}} \\ {}^{s}\boldsymbol{\tau_{o,k}} \end{bmatrix} - \begin{bmatrix} {}^{s}\boldsymbol{f_{nc,k}} \\ {}^{s}\boldsymbol{\tau_{nc,k}} \end{bmatrix} \tag{13}$$

For details on the estimation of force-torque sensor offsets please consult [14].

The previous paragraphs have focused on the *elimination* of non-contact forces-torques. If the non-contact forces-torques are to be *scaled* (cf. Fig. 2), ${}^{S}\boldsymbol{f_{nc}}$ ${}^{S}\boldsymbol{\tau_{nc}}$ have to be multiplied with a scaling constant $\sigma \neq 0$. σ controls the influence of the calculated non-contact forces and torques. Generally, two intervals and two special cases may be distinguished:

- $\sigma = 0$: The entire non-contact forces and torques are subtracted. This setting results in an apparently massless load.
- $0 < \sigma < 1$: The apparent mass m_a of the load ranges between zero $m_a = 0$ and the original mass $m_a = m$.
- $\sigma = 1$: No contact forces and torques are subtracted. The apparent mass equals the original mass, i.e., $m_a = m$.
- $1 < \sigma < \infty$: The apparent mass of the load is higher than the original mass, i.e., $m_a > m$.

Similarly, the parameter γ controls the magnitude of the contact forces-torques contained in the output ${}^{S}\boldsymbol{f'}$, ${}^{S}\boldsymbol{\tau'}$ (cf. Fig. 2) with $\gamma = 1$ leaving the contact forces-torques unchanged.

Since the inertia matrix of a complex body can be decomposed into the inertia matrices of its parts, the inertia matrices of a gripper or an end-effector and a gripped object may be separated thus enabling elimination or scaling of the non-contact forces and torques exerted by specific parts of the load. An important special case is the elimination of the non-contact forces-torques exerted by a gripper while preserving (a fraction $\eta \in [0, 1]$ of) those resulting from a gripped object. To facilitate this, a modified parameter vector ${}^{S}\hat{\boldsymbol{\varphi}}_{\boldsymbol{mod}}$ has to be employed in Eq. (12). Note that $\sigma = 0$ and $\gamma = 1$ must hold in this case or the structure in Fig. 2 has to be extended to incorporate this special case. Needless to say that the inertial parameters of the gripper have to be calculated or estimated beforehand to calculate the parameter vector of the gripped object ${}^{S}\hat{\boldsymbol{\varphi}}_{\boldsymbol{obj}}$. Let ${}^{S}\hat{\boldsymbol{I}}_{\boldsymbol{gr}}$ denote the inertia matrix of the gripper w.r.t. the sensor frame $\boldsymbol{S}$ and ${}^{S}\hat{\boldsymbol{I}}_{\boldsymbol{obj}}$ that of the gripped object. The modified parameter vector is then given by

$$ {}^{S}\hat{\boldsymbol{\varphi}}_{\boldsymbol{mod}} = {}^{S}\hat{\boldsymbol{\varphi}}_{\boldsymbol{gr}} + (1 - \eta)\, {}^{S}\hat{\boldsymbol{\varphi}}_{\boldsymbol{obj}} \tag{14}$$

.

VI. Experimental Results

To demonstrate the effectiveness of our approach, several experimental results are presented in the following. Before discussing the results, the first subsection will give a brief overview of our teleoperation system. In the second subsection, the elimination and scaling of non-contact forces and torques during free-space movements is discussed. In the third subsection, the elimination of non-contact forces-torques in contact transitions is addressed.

A. System Overview

Our teleoperator system consists of a Sensable Phantom Premium 1.5 HighForce/6DoF haptic device, a 6DoF Stäubli industrial manipulator (RX 60 or RX90) with a modified CS7B controller, and a combined 6DoF force-torque and 6DoF acceleration sensor JR3 85M35A3-I40-D 200N12. The joint position controllers of the slave run at a rate of $10kHz$, force-torque values may be sampled at rates of up to $8kHz$, and the haptic device may be operated at an update rate of more than $2kHz$ employing our own driver implementation for the QNX Neutrino RTOS. Fig. 3 shows an overview of the system hardware.

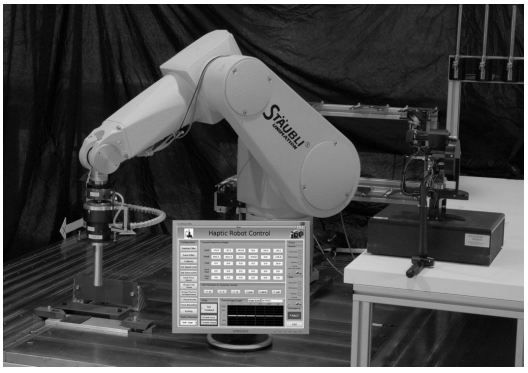

Fig. 3. Our teleoperation system consisting of a Stäubli RX90 manipulator, a Phantom 1.5 HighForce/6DoF haptic device, and a graphical user interface. Below the end-effector of the slave manipulator, surfaces with different stiffness values are shown.

Our teleoperator system is currently based on a position-force architecture [20], i.e., the pose of a haptic device (master) is used to control the pose of a slave manipulator and the forces-torques measured by the wrist-mounted force-torque sensor are fed back to the haptic device. The following brief description of the employed control approach is not intended to be a formal in-depth discussion of the employed control approach but will provide a basic understanding of

the structure of our system. Details of our teleoperation system can be found in [21]. Fig. 4 presents a structural overview.

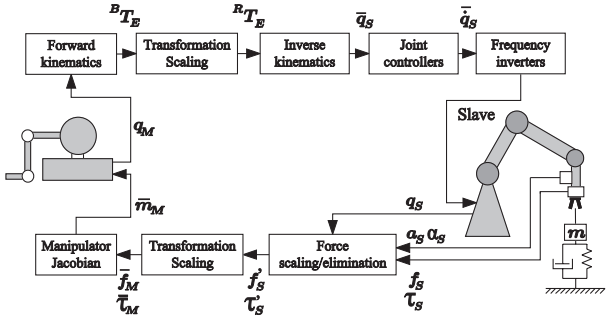

Fig. 4. Structural overview of the teleoperation system. The environment is illustrated by a mass-spring-damper system.

Starting at the master, the current joint angles of the master $\boldsymbol{q_M}$ are forwarded to the forward kinematics yielding the homogeneous transformation ${}^{B}\boldsymbol{T_E}$ relating the end-effector (stylus) of the master to the base. Before calculating the inverse kinematics of the slave, the translational and the rotational motion of the master may be scaled if desired. For orientation scaling quaternions are employed. The resulting transformation ${}^{R}\boldsymbol{T_E}$ relates the end-effector of the slave to its base. The joint angle setpoints $\bar{\boldsymbol{q}}_{\boldsymbol{S}}$ calculated by the inverse kinematics are then forwarded to the joint controllers. Joint velocities $\dot{\bar{\boldsymbol{q}}}_{\boldsymbol{S}}$ calculated by these controllers serve as input for the frequency inverters of the slave. The accelerations measured by the acceleration sensor (which is integrated in the force-torque sensor in our setup) and angular velocity signals derived from encoder measurements $\boldsymbol{q_S}$ are used to calculate the non-contact forces and torques employing the inertial parameters which have been estimated or calculated beforehand. These non-contact forces and torques are then subtracted from the forces $\boldsymbol{f_S}$ and torques $\boldsymbol{\tau_S}$ measured by the wrist-mounted force-torque sensor. Both the calculation of the non-contact forces and torques and the subtraction from the measured forces and torques according to Fig. 2 are performed in the 'Force scaling/elimination' block. The resulting forces and torques are subsequently scaled and transformed to the end-effector frame of the master device. Using the manipulator Jacobian $\boldsymbol{J_M}$ of the master, the joint torque setpoints $\bar{\boldsymbol{m}}_{\boldsymbol{M}}$ for the master are calculated based on $\bar{\boldsymbol{f}}_{\boldsymbol{M}}$ and $\bar{\boldsymbol{\tau}}_{\boldsymbol{M}}$, i.e., $\bar{\boldsymbol{m}}_{\boldsymbol{M}} = \boldsymbol{J}_{\boldsymbol{M}}^{\boldsymbol{T}} \left[\bar{\boldsymbol{f}}_{\boldsymbol{M}}, \bar{\boldsymbol{\tau}}_{\boldsymbol{M}}\right]^{T}$.

B. Elimination and Scaling of Non-Contact Forces and Torques in Free Space

This subsection addresses the scaling of non-contact forces and torques during free-space movements. Fig. 5 shows the force-torque and acceleration sensor as well as an end-effector with a ball tip. This end-effector has been employed in both the free space experiments in this subsection and the contact experiments discussed in Subsection VI-C.

The inertial parameters of the rigid object consisting of the end-effector and the sensor adapter have been estimated

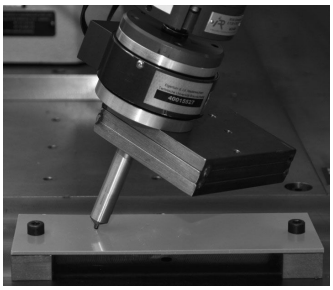

Fig. 5. Experimental tool and test environment. The tool consists of an adapter mounted on the force-torque sensor, a steel cuboid, and an aluminum rod with a ball tip. In the experiments presented in Subsection VI-C, the tool impacts on the sheet spring below it. Note that one support of the spring has been removed for this experiment. The experiments in Subsection VI-B do not involve any contacts with the environment.

on-line according to Section IV. The overall mass of the end-effector including the sensor adapter is $3.13kg$. Thus, if highly-dynamic movements are executed with the haptic device, significant non-contact forces and torques are exerted on the sensor. To prevent exceeding the maximum ratings of the Phantom device, the forces and torques exerted on the slave have been scaled down by a factor of 17.5 in the following experiments. Nevertheless, highly-dynamic teleoperation tasks may exhaust the operator after some time as may be inferred from the following experiments.

To evaluate the effectiveness of our approach during free-space movements, a rather fast vertical movement of the master stylus with the depicted orientation of the slave end-effector has been executed. In the first experiment, the scaling and elimination of non-contact forces is addressed; the second experiment presents results on torque scaling and elimination.

Using the estimated inertial parameters, the non-contact forces and torques exerted by the load can be calculated employing Eq. (4) and scaled or eliminated subsequently. All subplots in the following figures are scaled identically to stress the effectiveness of the approach. Note that in the following two figures the forces and torques resp. in the bottom plots serve as inputs for the haptic device (after downscaling). The top plot in Fig. 6 shows the measured force in one direction during a highly-dynamic vertical motion of the haptic device in free space. Although the forces are scaled down by a factor of 17.5, as already mentioned above, the user experiences considerable non-contact forces and torques, viz., up to approx. $5.7N$ when accelerating and decelerating the load. If loads with higher masses are employed, the resulting non-contact forces may be significant even in less dynamic situations. The middle plot in Fig. 6 shows the remaining force if the non-contact forces and torques are scaled down by a factor of $\sigma = 0.5$ thus resulting in half the mass of the original end-effector. The bottom plot shows the calculated contact force, i.e., the calculated non-contact forces have been fully removed from the measurements. The remaining force does never exceed $5N$ on the slave side. Thus, the user experiences a virtually massless object. Needless to say that the noticeable

inertia of the haptic device remains. Compared to the exerted non-contact forces and torques, the remaining disturbances present in the bottom plot are negligible, which significantly reduces operator fatigue.

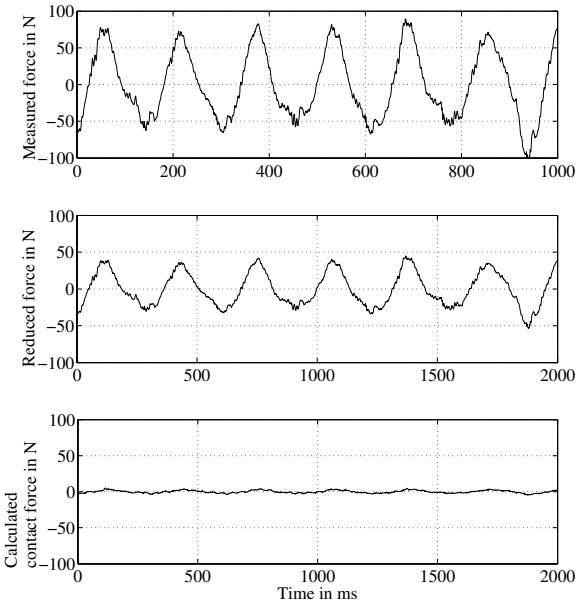

Fig. 6. Plots showing both scaling and elimination of non-contact forces. In the top plot, the force in one direction measured by the force-torque sensor is depicted. The middle plot shows the resulting force when the mass of the load is reduced to 50% by scaling the subtracted non-contact forces with a factor of $\sigma = 0.5$. In the bottom plot, the calculated non-contact forces have been fully removed from the measurements. As can be seen, only negligible disturbance forces remain.

Fig. 7 shows the scaling and elimination of non-contact torques in a corresponding experiment. In contrast to the previous experiment, a horizontal movement has been executed. As can be observed, the remaining torques in the bottom plot are very low which underpins the effectiveness of our approach. As in the previous case, the contact torque serves as input for the haptic device after downscaling.

C. Elimination of Non-Contact Forces and Torques in Contact Transitions

Fig. 8 shows the performance of our approach w.r.t. contact detection. A repetitive vertical movement has been executed. At $t \approx 220ms$, a contact with a sheet spring (cf. Fig. 5) is established. In the top plot, the measured force is depicted. The bottom plot shows the calculated contact force. As can be seen, the contact can clearly be spotted in the bottom plot whereas it is less obvious in the top plot. Similarly, the user does only perceive the contact if the non-contact forces and torques are eliminated. Note that at $t \approx 600ms$ no contact is established.

VII. Conclusion and Outlook

This paper proposes an approach to scaling or eliminating non-contact forces and torques, e.g., inertial forces,

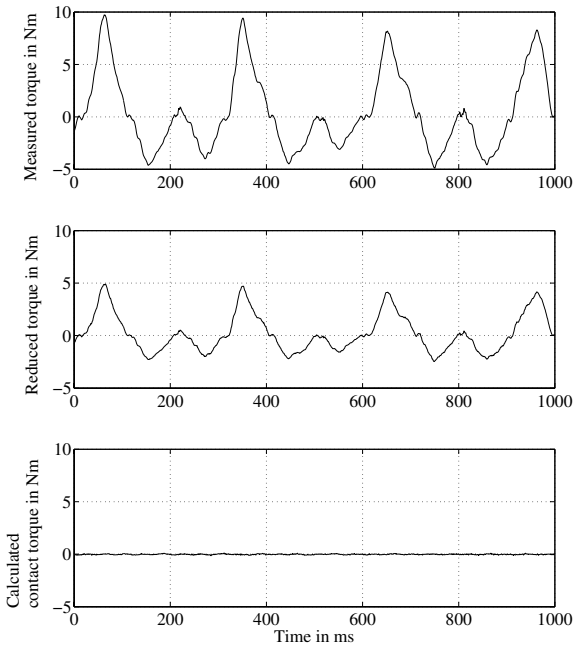

Fig. 7. Plots showing both scaling and elimination of non-contact torques. Similar to Fig. 6, in the top plot the measured torques are depicted; in the middle plot half of the calculated non-contact torque has been removed; in the bottom plot the non-contact torque has been fully removed leaving merely negligible disturbances.

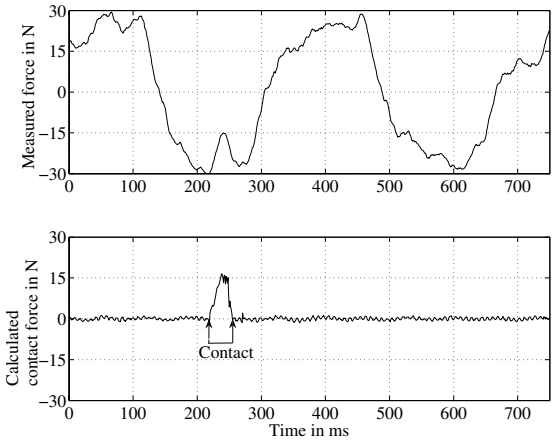

Fig. 8. The top plot shows the measured force involving contact with environment. The resulting contact force, however, is significantly lower than the inertial forces. Therefore, the user can hardly detect the contact. As can be seen in the bottom plot, removing the inertial forces from the measurements significantly simplifies the detection of the contact for both human users and contact detection algorithms.

centrifugal forces, Coriolis forces, and associated torques, in bilateral teleoperation applications. Using a 6DoF acceleration sensor, the calculation of these non-contact forces and torques, which are exerted onto the force-torque sensor of the slave, becomes feasible during teleoperation. The calculated non-contact forces-torques may then be

fully or partially subtracted(added) from(to) the force-torque measurements thus yielding contact forces-torques without or with reduced(increased) non-contact forces and torques respectively. Thus, our approach enables both scaling and zeroing the apparent mass of an end-effector, a gripper, or both a gripper and a manipulated object during teleoperation. Regarding the influence of the gripper, zeroing its non-contact forces-torques is desirable as a step towards transparency. Moreover, scaling or even eliminating the non-contact forces and torques of the entire load may be wise to decrease operator fatigue in highly-dynamic teleoperation applications and facilitate the detection of contacts with the environment. Without downscaling or eliminating non-contact forces and torques, contacts are perceived later or not at all depending on the type of contact. Although transparency is commonly regarded as a major design goal, maximum transparency might not be the optimal criterion when designing a teleoperation system for handling and assembly operations. Here, usability and performance during assembly tasks may be increased by scaling the non-contact and/or the contact forces and torques which are measured by a force-torque sensor (and would be sensed by the human when directly interacting with the environment). The effectiveness of our approach has been demonstrated in experiments regarding both free space movements and contact situations. A thorough psychophysical analysis has not been accomplished yet.

Ongoing and future research will focus on the psychophysical aspects of this approach. While the effectiveness of the approach has clearly been demonstrated in the presented experiments, user benefits – apart from reduced fatigue and better contact detection – have to be examined more closely from a psychophysical point of view. On the one hand, contact detection, which is impeded by non-contact forces-torques, is a key element in any assembly task; on the other hand, humans do consider inertial properties – especially the mass – of an object when mating it. Further experiments will show whether assembly tasks are performed faster or more accurately when inertial forces and associated torques are removed(scaled down). The user then experiences a massless(lighter) object but may be able to detect contacts earlier. Thus, the question arises how non-contact forces-torques and contact forces-torques have to be scaled to optimize assembly performance. For instance, reducing the apparent mass and increasing the perceived contact force may yield an improved assembly performance.

ACKNOWLEDGMENTS

We would like to thank *QNX Software Systems* for providing free software licenses. Moreover, we are indebted to Torsten Kröger, who designed our robot control architecture as well as Ingo Weidauer and Francisco Rey Portero who contributed to our teleoperation system. Furthermore, we would like to thank Harald Meyer-Kirk for manufacturing all mechanical accessories.

REFERENCES

[1] P. F. Hokayem and M. W. Spong. Bilateral teleoperation: An historical survey. *Automatica*, 42(12):2035–2057, December 2006.

[2] L. A. Jones and S. J. Lederman. *Human Hand Function*. Oxford University Press, 2006.

[3] S. Choi and H. Z. Tan. An experimental study of perceived instability during haptic texture rendering: Effects of collision detection algorithm. In *Proceedings of the 11th Symposium on Haptic Interfaces for Virtual Environment and Teleoperator Systems (HAPTICS03)*, pages 197–204, 2003.

[4] C. Preusche, G. Hirzinger, J. H. Ryu, and B. Hannaford. Time domain passivity control for 6 degrees of freedom haptic displays. In *Proc. of IEEE/RSJ International Conference on Intelligent Robots and Systems*, pages 2944–2949, 2003.

[5] M. Mahvash and A. M. Okamura. Enhancing transparency of a position-exchange teleoperator. In *Proceedings of Second Joint Euro-Haptics Conference and Symposium on Haptic Interfaces for Virtual Environment and Teleoperator Systems (WHC'07)*, 2007.

[6] M. Mahvash, J. Gwilliam, R. Agarwal, B. Vagvolgyi, L.-M. Su, D. D. Yuh, and A. M. Okamura. Force-feedback surgical teleoperator: Controller design and palpation experiments. In *Proceedings of Symposium on Haptic Interfaces for Virtual Environments and Teleoperator Systems 2008*, pages 465–471, 2008.

[7] D. Lee and P. Y. Li. Passive bilateral control and tool dynamics rendering for nonlinear mechanical teleoperators. *IEEE Trans. on Robotics*, 21(5):936–951, October 2005.

[8] D. Kubus, T. Kröger, and F. M. Wahl. On-line rigid object recognition and pose estimation based on inertial parameters. In *Proc. of IEEE/RSJ International Conference on Intelligent Robots and Systems*, pages 1402–1408, 2007.

[9] D. Kubus, T. Kröger, and F. M. Wahl. On-line estimation of inertial parameters using a recursive total least-squares approach. In *Proc. of IEEE/RSJ International Conference on Intelligent Robots and Systems*, pages 3845–3852, 2008.

[10] K. Kozlowski. *Modelling and Identification in Robotics*. Advances in Industrial Control. Springer, 1998.

[11] J. Gámez García, A. Robertsson, J. Gómez Ortega, and R. Johansson. Force and acceleration sensor fusion for compliant robot motion control. In *Proc. of IEEE International Conference on Robotics and Automation*, pages 2709–2714, 2005.

[12] J. Gámez García, A. Robertsson, J. Gómez Ortega, and R. Johansson. Generalized contact force estimator for a robot manipulator. In *Proc. of IEEE International Conference on Robotics and Automation*, pages 4019–4024, 2006.

[13] T. Kröger, D. Kubus, and F. M. Wahl. 6D force and acceleration sensor fusion for compliant manipulation control. In *Proc. of IEEE/RSJ International Conference on Intelligent Robots and Systems*, pages 2626–2631, 2006.

[14] D. Kubus, T. Kröger, and F. M. Wahl. Improving force control performance by computational elimination of non-contact forces/torques. In *Proc. of IEEE International Conference on Robotics and Automation*, 2008.

[15] P. J. McKerrow. *Introduction to Robotics*. Addison-Wesley Publishers Ltd., 1991.

[16] J. Swevers, C. Ganseman, D. B. Tükel, J. de Schulter, and H. Van Brussel. Optimal robot excitation and identification. *IEEE Trans. on Robotics and Automation*, 13(5):730–739, 1997.

[17] J. Swevers, W. Verdonck, B. Naumer, S. Pieters, and E. Biber. An experimental robot load identification method for industrial application. *The International Journal of Robotics Research*, 21(8):701–712, 2002.

[18] P. R. Belanger. Estimation of angular velocity and acceleration from shaft encoder measurements. In *Proc. of IEEE International Conference on Robotics and Automation*, 1992.

[19] T. Kröger, D. Kubus, and F. M. Wahl. 12d force and acceleration sensing: A helpful experience report on sensor characteristics. In *Proc. of IEEE International Conference on Robotics and Automation*, 2008.

[20] Günter Niemeyer, Carsten Preusche, and Gerd Hirzinger. *Handbook of Robotics*, chapter 31, pages 741–755. Springer, 2008.

[21] D. Kubus, I. Weidauer, and F. M. Wahl. 1khz is not enough — how to achieve higher update rates with a bilateral teleoperation system based on commercial hardware. In *Proc. of IEEE/RSJ International Conference on Intelligent Robots and Systems*, 2009.